AD-A145 745 THREE ARTICLES ON NEW CALCULATION METHODS IN AERONAUTICS (SELECTED ARTICLES)(U) FOREIGN TECHNOLOGY DIV WRIGHT-PATTERSON AFB OH F DEXUN ET AL. 17 AUG 84 1/1

UNCLASSIFIED FTD-ID(RS)T-0910-84 F/G 20/4 NL

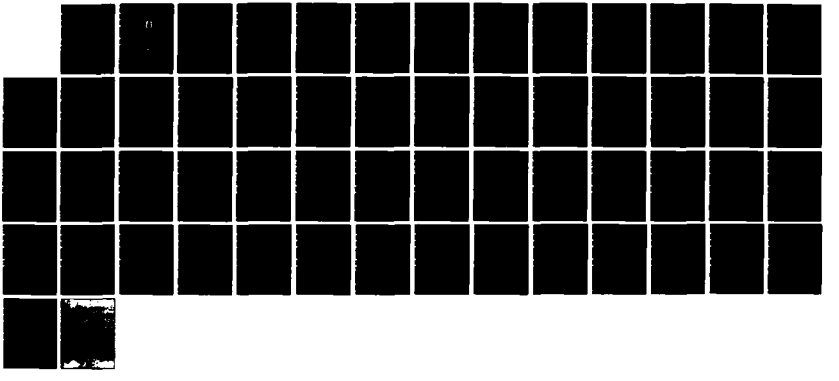

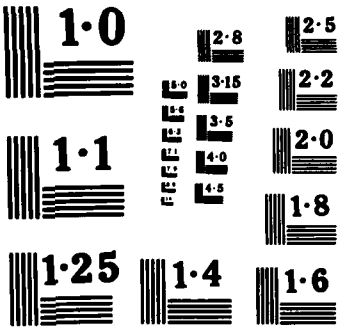
1·0
1·1
1·25
1·4
1·6
1·8
2·0
2·2
2·5
2·8
3·15
3·5
4·0
4·5

FTD-ID(RS)T-0910-84

FOREIGN TECHNOLOGY DIVISION

THREE ARTICLES ON NEW CALCULATION METHODS IN AERONAUTICS
(Selected Articles)

Approved for public release;
distribution unlimited.

EDITED TRANSLATION

FTD-ID(RS)T-0910-84 17 Aug 1984

MICROFICHE NR: FTD-84-C-000815

THREE ARTICLES ON NEW CALCULATION METHODS IN AERONAUTICS
(Selected Articles)

English pages: 50

Source: Hangkong Xuebao, Vol. 4, Nr. 3, September 1983, pp. 1-8; 9-18; 56-62; 102-104

Country of origin: China
Translated by: LEO KANNER ASSOCIATES
F33657-81-D-0264
Requester: FTD/TQTA

PREPARED BY:

TRANSLATION DIVISION
FOREIGN TECHNOLOGY DIVISION
WP-AFB, OHIO.

Table of Contents

GRAPHICS DISCLAIMER

All figures, graphics, tables, equations, etc. merged into this translation were extracted from the best quality copy available.

NUMERICAL SOLUTION OF HYPERSONIC FLOW NEAR LEADING EDGE OF A FLAT PLATE

Fu Dexun
Beijing Institute of Aerodynamics

Abstract

This paper uses a one step difference scheme with second-order accuracy in space for the numerical solution of Navier-Stokes equations as brought forth in Reference [1] to numerically calculate the transonic and hypersonic interaction problems near the leading edge of a flat plate. The scheme is discussed and analyzed with simple model equations. We used this method to calculate the interaction problems of the leading edge of a flat plate with M_∞ =20, $\overline{T}_W/\overline{T}_O$=0.06, $Re_{\infty\ L}$=4x10^3 and M_∞ =3, $\overline{T}_W$=$\overline{T}_O$, and $Re_{\infty\ L}$=10^3.

The calculation results accord well with the test results and with these results we can more clearly understand the flow characteristics of the interaction near the leading edge of a flat plate.

I. Introduction

What we are interested in here is a steady-state solution for the interaction problems near the leading edge of a flat plate. Starting from the use of non-steady-state partially differential equations to solve its steady-state problems is the simplest iteration method. Being that the steady-state solution is necessary, the solution process then does not require a solution corresponding to the original non-steady-state partially differential equations but it is only necessary that the stabilized solution approach the solution of the steady-state problems. This gives the structural difference scheme a certain amount of flexibility. This paper proposes an improved

iteration scheme based on the non-steady-state equations. It is a one-step scheme and does not approximate the original non-steady-state differential equations. Yet its stabilized solution has second order accuracy in space. It can be known through analysis that the stable conditions of this scheme are more relaxed than those of most explicit schemes and it is even simpler than the commonly used two-step difference scheme. This paper uses this method to calculate the interaction problems of the leading edges of dual flat plates.

In the last several years, many theories have appeared and a great deal of research has been done on the hypersonic flow around the leading edge of a flat plate [1,8]. Test results show that in the hypersonic flow around a pointed flat plate, there exists a very small non-continuous flow region near the leading edge of the flat plate. This region uses the quantity of the molecular average free path and quantum level as the characteristic length. This region is closely connected into a continuous flow region. In this region, the shock wave layer and boundary layer are completely mixed together and we call it the merged layer region. After the continuous flow region is there, it is a weak interaction region and here the viscous region near the wall surface and the non-viscous region of the outer surface can clearly be divided into two layers. Therefore, the classical boundary layer theory can be used in the weak interaction region. Following the enlargement of the incident flow's Mach number M_∞ and the decrease of the Reynolds number, the merged layer region enlarges.

If we introduce interaction parameter $X=c^{1/2}M_\infty^3/(Re_{\infty L})^{1/2}$ (c is the Chapman viscous constant), the $X_\infty \to 0$ is in the weak interaction region as well as in the strong interaction region $X_\infty \gg 1$.

It has already been pointed out that the shock wave layer is completely mixed together with the boundary layer in the merged

layer region and therefore use of the general boundary layer theory cannot be described. In order to obtain an even better theoretical calculation method, S.G. Rubin et al carried out detailed quantitative analysis of steady-state Navier-Stokes equations in different flow regions and gave simplified Navier-Stokes equations suitable for the entire continuous flow region. Moreover, they used the difference method to numerically solve this set of simplified steady-state partially differential equations. The computation results are given in Reference [2]. The calculation results of Rubin et al are greatly improved as compared to the results from the strong interaction theory yet in order to solve the set of simplified steady-state partially differential equations, it is necessary to give the initial conditions (i.e. the incident flow boundary conditions) on a certain section of the leading edge of the flat plate and the corresponding boundary conditions. In this way, the computation results more strongly rely on the conditions on the upstream initial section and the differences of the results of different upstream conditions are very large. This paper employs the method in Reference [1] and gives the results of the supersonic and hypersonic flows around flat plates. The computation field is shown in Fig. 2. The difference schemes is established based on the non-steady-state Navier-Stokes equations and uses the initial value the moment the uniform incident flow is t=0. The upstream boundary is selected at a certain distance on the leading edge of the flat plate and we also select the uniform incident flow as the boundary condition. In this way, we avoid the drawback of the method proposed by Rubin et al.

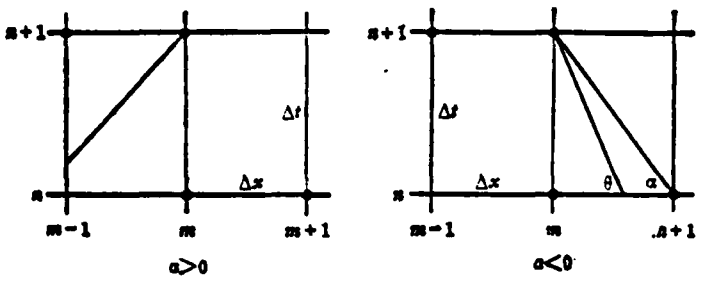

Fig. 1 Schematic representation of the network.

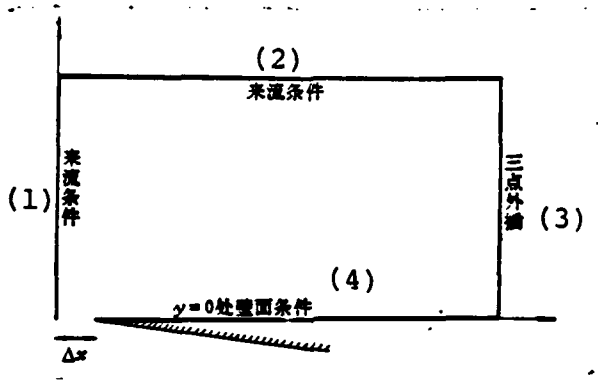

Fig. 2 Computational field.

Key: (1)-(2) Incident flow conditions; (3) Three-point extrapolation; (4) Wall surface conditions in y=0 area.

The second part of this paper uses model equations to give the difference scheme, the third part gives the two-dimensional Navier-Stokes equations and their difference approximation formulas and lastly gives the numerical computation results of the interaction problems for the leading edge of the flat plate.

II. Difference Scheme

For the purpose of simplification, we discuss the following model equation

$$\frac{\partial u}{\partial t} = \nu \frac{\partial^2 u}{\partial x^2} - a \frac{\partial u}{\partial x} \qquad (1)$$

In the formula, v and a are constants. Here, we use the second-order derivative term in space to simulate the viscous term in in the Navier-Stokes equation and use the first order derivative in space to simulate the convection term. It is necessary that we satisfy the steady-state solution of equation (1) which has certain boundary conditions. We use the following difference scheme of Reference [1] for equation (1)

$$u_m^{n+1}=u_m^n+\Delta t\left[\nu\frac{u_{m+1}^n-2u_m^n+u_{m-1}^{n+1}+2\beta(u_m^n-u_m^{n+1})}{\Delta x^2}-a\frac{u_{m+1}^n-u_{m-1}^{n+1}}{2\Delta x}\right] \qquad (2)$$

This difference equation uses second-order accuracy to approximate the following differential equation

$$\frac{\partial u}{\partial t}+K\left(a\frac{\partial u}{\partial x}-\nu\frac{\partial^2 u}{\partial x^2}\right)=0 \qquad (3)$$

In the equation

$$K=\frac{1}{1-\frac{\Delta t}{\Delta x}\left[\nu\frac{(1-2\beta)}{\Delta x}+\frac{a}{2}\right]} \qquad (4)$$

It can be seen that when $\frac{\partial u}{\partial t}=0$, equations (3) and (1) correspond to the same type of steady-state equation. It is very obvious that when $K<0$, the formulation of the problem is not suitable. This is because at this time, as regards the viscous term, the problem of reverse heat conduction arises and changes the characteristic trend of the convection term (the characteristic values a and Ka have different symbols). Therefore, in order to be able to obtain the asymptotic solution when time t is quite large, the necessary condition is $K\geqslant 0$, that is

$$\frac{\Delta t}{\Delta x}\left[\nu\frac{1-2\beta}{\Delta x}+\frac{a}{2}\right]\leqslant 1 \qquad (5)$$

Below, we will discuss the stability conditions. Under $K>0$ conditions, when $a>0$, then $Ka>0$ and at this time the dependent area of difference equation (2) always includes the

dependent area of differential equation (3). If we only consider the convection term, difference equation (2) is always steady. When $a < 0$, the $-Ka > 0$ (here, it is still necessary that $K > 0$, that is that the conditions in equation (5) are satisfied). At this time, in order to cause the dependent area of difference equation (2) to include the dependent area of the differential equation, it is necessary that $\Delta t/\Delta x \leqslant -1/Ka$ (see Fig. 1), that is

$$\frac{\Delta t}{\Delta x}\left[\nu\frac{1-2\beta}{\Delta x}-\frac{a}{2}\right]\leqslant 1 \qquad (6)$$

By synthesizing equations (5) and (6), we can obtain the stable conditions of difference equation (2):

$$\frac{\Delta t}{\Delta x}\left[\nu\frac{1-2\beta}{\Delta x}+\frac{|a|}{2}\right]\leqslant 1 \qquad (7)$$

When $\beta=1/2$, the above stable conditions become

$$|a|\frac{\Delta t}{\Delta x}\leqslant 2 \qquad (8)$$

By comparing equation (8) and Courant condition $|a|\ \frac{\Delta t}{\Delta x}\leqslant 1$, we can see that when taking $\beta=1/2$, the difference scheme (2) will doubly widen the limitation of the stable conditions towards step-length ratio $\Delta t/\Delta x$.

III. The Fundamental Equations and Their Difference Approximations

1. The Fundamental Equations

In the cartesian coordinate system, the non-conservative type two-dimensional Navier-Stokes equation has the following form after nondimensionalization [1]

$$\frac{\partial U}{\partial t}+A_1\frac{\partial U}{\partial x}+A_2\frac{\partial U}{\partial y}=S \qquad (9)$$

Here, U and S are vectors, and A_1 and A_2 are matrices

$$U=\begin{pmatrix}\rho\\ u\\ v\\ T\end{pmatrix} \qquad S=\begin{pmatrix}s_1\\ s_2\\ s_3\\ s_4\end{pmatrix}$$

$$A_1=\begin{pmatrix} u & \rho & 0 & 0\\ \frac{1}{\gamma M_\infty^2}\frac{T}{\rho} & u & 0 & \frac{1}{\gamma M_\infty^2}\\ 0 & 0 & u & 0\\ 0 & (\gamma-1)T & 0 & u\end{pmatrix}$$

$$A_2=\begin{pmatrix} v & 0 & \rho & 0\\ 0 & v & 0 & 0\\ \frac{T}{\gamma M_\infty^2\rho} & 0 & v & \frac{1}{\gamma M_\infty^2}\\ 0 & 0 & (\gamma-1)T & v\end{pmatrix}$$

$$s_1=0$$

$$s_2=\frac{1}{\rho}\left(\frac{\partial\sigma_{11}}{\partial x}+\frac{\partial\sigma_{13}}{\partial y}\right)$$

$$s_3=\frac{1}{\rho}\left(\frac{\partial\sigma_{13}}{\partial x}+\frac{\partial\sigma_{33}}{\partial y}\right)$$

$$s_4=\frac{1}{\rho}\frac{\gamma}{Re_{\infty L}Pr}\left[\frac{\partial}{\partial x}\mu\frac{\partial T}{\partial x}+\frac{\partial}{\partial y}\mu\frac{\partial T}{\partial y}\right]$$

$$+\frac{1}{\rho c_v}\left[\sigma_{11}\frac{\partial u}{\partial x}+\sigma_{13}\frac{\partial v}{\partial x}+\sigma_{13}\frac{\partial u}{\partial y}+\sigma_{33}\frac{\partial v}{\partial y}\right]$$

$$\sigma_{11}=\frac{2\mu}{Re_{\infty L}}\left(\frac{\partial u}{\partial x}-\frac{1}{3}\mathrm{div}V\right)$$

$$\sigma_{13}=\frac{\mu}{Re_{\infty L}}\left(\frac{\partial u}{\partial y}+\frac{\partial v}{\partial x}\right)$$

$$\sigma_{33}=\frac{2\mu}{Re_{\infty L}}\left(\frac{\partial v}{\partial y}-\frac{1}{3}\mathrm{div}V\right)$$

$$\mathrm{div}V=\frac{\partial u}{\partial x}+\frac{\partial v}{\partial y}$$

When there is nondimensionalization, the reference parameters are separately: $x=\bar{x}/L$, $y=\bar{y}/L$, $t=\bar{t}\bar{U}_\infty/L$, $\rho=\bar{\rho}/\bar{\rho}_\infty$, $T=\bar{T}/\bar{T}_\infty$, $p=\bar{p}/\bar{U}_\infty^2\bar{\rho}_\infty$, $u=\bar{u}/\bar{U}_\infty$, $v=\bar{v}/\bar{U}_\infty$, $\mu=\bar{\mu}/\bar{\mu}_\infty$ and L is the length of the flat plate. After nondimensionalization, the state equation is

$$p=\frac{1}{\gamma M_\infty^2}\rho T \tag{10}$$

We also have

$$c_v=\frac{p}{\gamma-1} \tag{11}$$

$$c_p=\gamma c_v \tag{12}$$

The coefficient of viscosity uses the Sutherland relational formula

$$\mu=\frac{c_1 T^{3/2}}{T+c_2}$$

In the formula

$$c_1=1+\frac{\bar{c}_2}{\bar{T}_\infty},\quad c_2=\frac{\bar{c}_2}{\bar{T}_\infty},\quad \bar{c}_2=114^\circ K$$

2. The Difference Equations

Using the difference scheme given in the previous section and taking $t=n\Delta t$, $x_1=i\Delta x$ and $y_j=j\Delta y$, then the difference equation corresponding to the set of equations in (9) have the following form

$$\frac{U_{i,j}^{n+1}-U_{i,j}^n}{\Delta t}+(A_1)_{i,j}^n\frac{U_{i+1,j}^n-U_{i-1,j}^{n+1}}{2\Delta x}+(A_2)_{i,j}^n\frac{U_{i,j+1}^n-U_{i,j-1}^{n+1}}{2\Delta y}=S_{i,j}^n \tag{13}$$

The second-order derivative term in $S_{i,j}^n$ (for example, $\frac{\partial}{\partial x}$ a $\frac{\partial u}{\partial x}$ and $\frac{\partial}{\partial x}$ a $\frac{\partial u}{\partial y}$)can use the following form of difference approximation

$$\frac{\partial}{\partial x}\,a\,\frac{\partial u}{\partial x}=\frac{1}{\Delta x^2}\left[a^n_{i+1/2,j}u^n_{i+1,j}-(a^n_{i+1/2,j}+a^n_{i-1/2,j})u^n_{i,j}+a^n_{i-1/2,j}u^{n+1}_{i-1,j}\right.$$
$$\left.+\beta\,(a^n_{i+1/2,j}+a^n_{i-1/2,j})(u^n_{i,j}-u^{n+1}_{i,j})\right]$$

$$\frac{\partial}{\partial x}\,a\,\frac{\partial u}{\partial y}=\frac{1}{4\Delta x\Delta y}\left[a^n_{i+1,j}(u^n_{i+1,j+1}-u^n_{i+1,j-1})-a^n_{i-1,j}(u^{n+1}_{i-1,j+1}-u^{n+1}_{i-1,j-1})\right]$$

We can carry out similar difference approximations for other second-order derivatives of function u as well as the second-order derivatives of other functions. In the difference equations, coefficients $a_{i\pm1/2,j}$ and $a_{i,j\pm1/2}$ are separately

$$a_{i\pm1/2,j}=\frac{1}{2}(a_{i,j}+a_{i\pm1,j})$$

$$a_{i,j\pm1/2}=\frac{1}{2}\,(a_{i,j}+a_{i,j\pm1})$$

3. The Boundary Conditions

The wall surface conditions in the y=0 area.

The non-slip flow conditions:

$$T=T_w,\quad u=v=0$$

$$p_w=\frac{1}{3}(4p_1-p_2)$$

Here, the lower symbols of 1 and 2 indicate the first and second points of the adjacent substance surface. The slip flow conditions:

$$v=0,\quad u=\lambda\frac{\partial u}{\partial y}$$

$$T=T_w+\frac{2\gamma}{1+\gamma}\,\frac{1}{P_r}\left(\lambda\frac{\partial T}{\partial y}\right)$$

In the equations, λ is the molecule's mean level of freedom.

The downstream boundary uses the three-point extrapolation formula

$$U_{I,J} = 3U_{I-1,J} - 3U_{I-2,J} + U_{I-3,J}$$

The lower symbol I indicates the last point of the downstream in the x direction (see Fig. 2).

IV. Computation Results

Based on the computation method proposed above, this paper calculated the flow interaction problems of the leading edge of the flat plate. We give two sets of computation results here. The first set of parameters is $M_\infty = 20$, $\bar{T}_W/\bar{T}_O = 0.06$, $\bar{T}_O = 9000°R$ and $Re_{\infty L} = 4 \times 10^3$; the second set of parameters is $M_\infty = 3$, $\bar{T}_W/\bar{T}_O = 1$ and $Re_{\infty L} = 10^3$. In order to overcome the false jumping in the numerical solution when there are super shock waves near the leading edge of the flat plate, in the calculations, we divided the entire flat plate into two sections in the x direction and used the calculation of $M_\infty = 3$ as an example. The first section was $-0.005 \leqslant x \leqslant 0.05$ and the second section was $0.0333 \leqslant x \leqslant 1.0$. In the first section, we used the step length Reynolds number $Re_{\Delta x} = 5$, $\Delta y/L = 0.005$; in the second section, we used $\Delta x/L = 0.048$, $(\Delta y/L)_{max} = 0.027$, $(\Delta y/L)_{min} = 0.02$. In the calculations of $M_\infty = 20$, we used the filter method. The selection of the computational field and boundary conditions was as shown in Fig. 2. We will now briefly present the computation results as follows:

1. Interaction Computations of the Leading Edge of a Flat Plate With $M_\infty = 20$

In the computations, the slip flow conditions were used on the surface and the density on the surface used the extrapolation value of the internal adjacent three points. The results of the computations are given in Figs. 3-5.

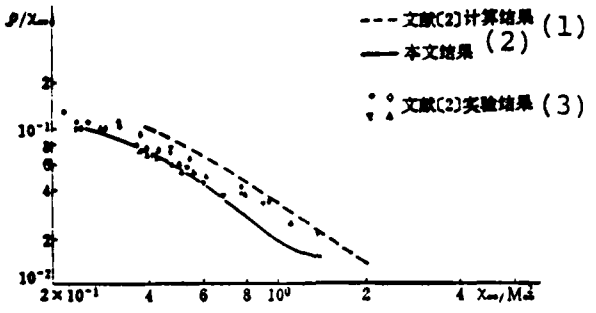

Fig. 3 Surface pressure distribution ($\overline{T}_W/\overline{T}_O$=0.06, M_∞ =20, $Re_{\infty L}$=4x10^3).

Key: (1) Computation results of Reference [2]; (2) Results of this paper; (3) Test results of Reference [2].

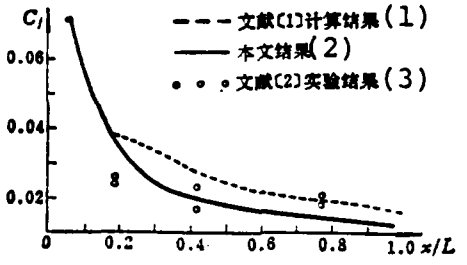

Fig. 4 Surface frictional resistance coefficient ($\overline{T}_W/\overline{T}_O$=0.06, M_∞ =20, $Re_{\infty L}$= 4x10^3).

Key: (1) Computations results of Reference [1]; (2) Results of this paper; (3) Test results of Reference [2].

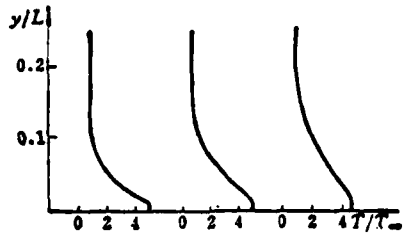

Fig. 5 Temperature profile ($\bar{T}_W/\bar{T}_0$=0.06, M_∞=20, $Re_{\infty L}$=4x10^3).

It can be seen from the computation results that the computation results of the merged layer field of the hypersonic flow near the leading edge of the flat plate given by the method of this paper accords well with the test values. It is difficult to give these kinds of results when using the strong interaction theory. Because we did not make any approximation assumptions but used the numerical computation method to directly solve the complete Navier-Stokes equations, we more accurately described the flow characteristics of the merged layer.

2. Computations of Flow Around Flat Plate With M_∞=3 and $Re_{\infty L}$=10^3

In this set of computations, we took pressure p_W=1/3(4p_1-p_2). In the formula, lower symbols 1 and 2 indicate the first and second points closest to the substance surface. Figures 6-8 give the computation results of this set. It can be seen from the figures that when Mach number M_∞ is not very large in the incident flow, the influence of using the non-slip flow surface conditions is not large on the downstream computations and that the computation results coincide with the results given by the weak interaction theory.

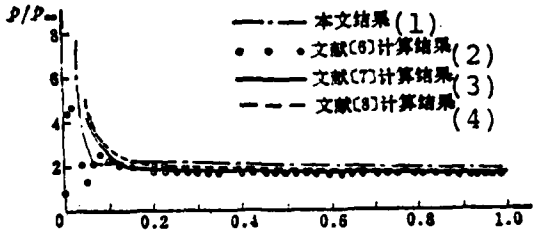

Fig. 6 Surface pressure distribution chart ($\overline{T}_W / \overline{T}_{O,\infty} = 1$, $M_\infty = 3$, $Re_{\infty L} = 10^3$).

Key: (1) Results of this paper; (2) Computation results of Reference [6]; (3) Computation results of Reference [7]; (4) Computation results of Reference [8].

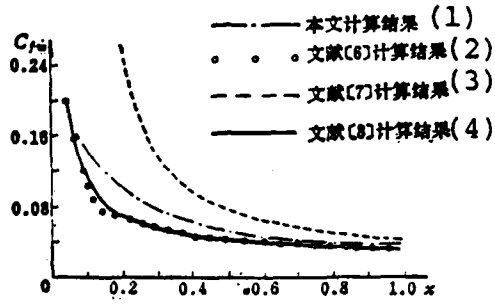

Fig. 7 Surface frictional resistance coefficient ($\overline{T}_W / \overline{T}_{O,\infty} = 1$, $M_\infty = 3$, $Re_{\infty L} = 10^3$).

Key: (1) Computation results of this paper; (2) Computational results of Reference [6]; (3) Computation results of Reference [7]; (4) Computation results of Reference [8].

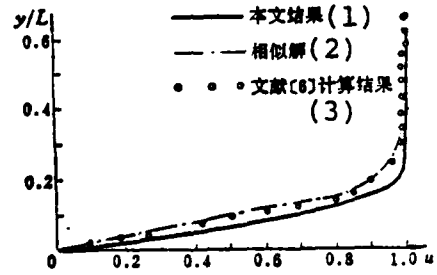

Fig. 8 Velocity profile ($T_W / T_{O,\infty} = 1$, $M_\infty = 3$, $Re_{\infty L} = 10^3$).
(continued next page)

Fig. 8 (continued)

Key: (1) Results of this paper; (2) Similar solution; (3) Computation results of Reference [6].

Use of the numerical computation method to solve the entire Navier-Stokes equations can allow us to better understand the flow characteristics of interaction near the leading edge of a flat plate.

References

[1] Fu Dexun, One-Step Difference Scheme With Second-Order Accuracy For Numerically Solving Navier-Stokes Equations, Report of the Beijing Institute of Aerodynamics, 1979.

[2] Rudman, S. and Rubin, S.G., Hypersonic Viscous Flow over Slender Bodies with Sharp Leading Edges, AIAA J.,No.10(1968).

[3] Nagamatsu, H.T., Sheer, R.E. and Schmid, J.R.,High Temperature Rarefield Hypersonic Flow over a Flat Plate, ASR J., 31(1961), 7.

[4] Nagamatsu, H.T. and Sheer, R.E., Hypersonic Shock Wave-Boundary Layer Interaction and Leading Edge Slip, ASR J., 30(1960), 5.

[5] Laurmann, J.A., The Free Molecular Probe and its Use for the Study of Leading Edge Flow. The Physics of Fluids, 1(1958).

[6] Carter,J.E., Numerical Solution of the Navier-Stokes Equations for the Supersonic Laminar Flow over a Two-Dimensional Compression Corner. NASA TR R-385.

[7] Lees, Lester and Probstein, R.F., Hypersonic Viscous Flow over a Flat Plate, Hypersonic Flow Theory, Academic Press Inc., 1959, pp 333-374.

[8] Kubota, Toshi and Ko, Denny, R.S., A Second-order Weak Interaction Expansion for Moderately Hypersonic Flow Past a Flat Plate, AIAA J., 5(1967), 5.

A NEW METHOD FOR CALCULATING UNSTEADY SUPERSONIC AERODYNAMIC FORCES AND ITS APPLICATION

Wang Xianxin
Chinese Aerodynamic Research and Development Center

Abstract

This paper proposes a new method for calculating supersonic unsteady aerodynamic forces. It combines the piston theory for unsteady supersonic flow with the conical flow theory for steady flow so that the interaction between points on a wing neglected in the piston theory is approximated by the conical flow theory. This method was used in this paper for flutter calculations of 29 cases for wings with 10 different types of plane forms. The results were compared with flutter test results obtained in wind tunnels and they were in satisfactory agreement. It was especially the case that the accuracy of flutter analysis improved by this method was noticeably higher than that obtained by the piston theory. This shows that this method is reliable and feasible for supersonic flutter analysis. It possesses the advantages of being a more succinct method and having higher calculation accuracy, less computing time and easier programming.

I. Introduction

The calculation of the supersonic unsteady aerodynamic forces and the flutter analysis of aircraft parts is tedious, time-consuming and yet indispensable work. At present, the commonly used numerical calculation methods are: the influence coefficient or M box method [1], the supersonic kernel function method [2] as well as the supersonic doublet grid method [3] etc. These methods use the ternary linearized potential theory as the basis and although they provide satisfactory accuracy when used yet none consume a great deal of computing time. An even more

commonly used simple and convenient method is the piston theory method [4]. The practice of flutter calculations shows the calculation accuracy of the piston theory is sometimes very good and sometimes very poor. Therefore, the raising of the calculating accuracy of the piston theory to develop a simple and convenient method which has satisfactory calculating accuracy and does not require a great deal of computing time is of real significance.

This paper proposes a new method for calculating supersonic unsteady aerodynamic forces. This method is formed by combining the piston theory with the conical flow theory for supersonic steady flow. The essence of the theory is: the interaction between the points on a wing neglected in the piston theory is approximated by the conical flow theory or we use the piston theory for dynamic frequency revisions and extend the conical flow theory for steady flow to non-steady conditions. In this paper, we carried out over 300 flutter analysis calculations of 29 conditions of 10 wings with different types of plane forms (delta wings, uniform chord wings, pointed swept-back wings and trapezoidal wings), checked this method and compared it with the flutter test results obtained in wind tunnels. Comparisons showed that the vast majority of calculations were in agreement with the wind tunnel test data especially when compared with the flutter analysis carried out by the piston theory wherein the accuracy was much higher. This shows that this method is reliable and feasible for supersonic flutter analysis. It has the advantages of being a succinct method and having higher accuracy, less computing time and easier programming.

II. General Outline of the Method

The interaction of the points on a wing is neglected by the piston theory and the simple harmonic aerodynamic forces caused by the airfoil thickness and the wing surface's unsteady movement is

$$P_e(x,\ y;\ \omega) = -2\rho a\left(i\omega + V\frac{\partial}{\partial x} + \frac{\gamma+1}{4a}\frac{\partial h}{\partial x}\left(i\omega V + V^2\frac{\partial}{\partial x}\right)\right)W(x,\ y) \qquad (1)$$

In the formula, ω is the vibration frequency on the wing surface; ρ is the air flow density; a is the speed of sound; V is the velocity of the incident flow; γ is the specific heat ratio; h is the airfoil thickness; W(x,y) is the wing surface's normal displacement.

The conical flow theory is a unique method for solving linearized supersonic steady flows. It gives the aerodynamic load on the wing surface as

$$P_e(x,\ y) = -2\rho V u \qquad (2)$$

When there is a subsonic leading edge, disturbance velocity u is (see Fig. 1(a)

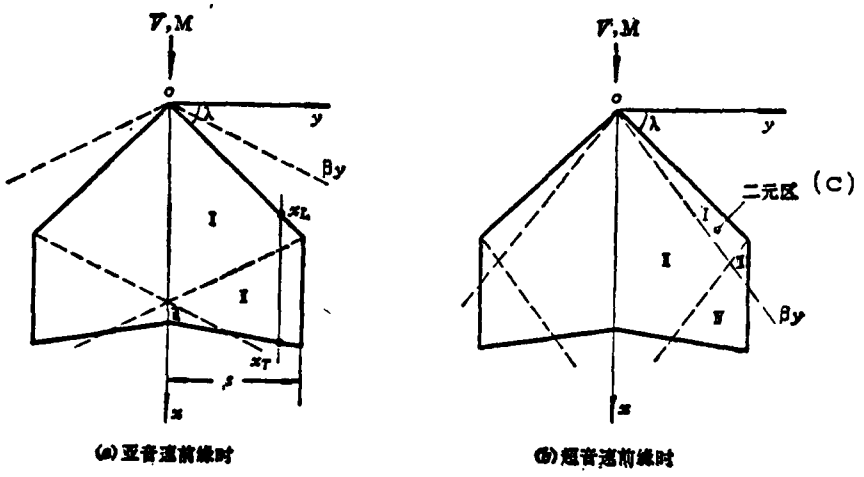

Fig. 1 Coordinate system and division of wing region.

Key: (a) When there is a subsonic leading edge; (b) When there is a supersonic leading edge; (c) Two-dimensional region.

Region I

$$u = u_{s1}(a_0) = \frac{m^2 V}{E'(m)\sqrt{m^2 - a_0^2}} \frac{\partial W(x, y)}{\partial x} \tag{3a}$$

Region II

$$u = u_{s2} = u_{s1}(a_1)\left(1 - \sqrt{\frac{(m + a_1)(1 + a_1)}{2m(m+1)}}\right) \tag{3b}$$

Region III

$$u = u_{s2} - u_{s1}(a_2)\sqrt{\frac{(m + a_2)(1 + a_2)}{2m(m+1)}} \tag{3c}$$

When there is a supersonic leading edge, disturbance velocity u is (see Fig. 1(b)).

Region I

$$u = u_{p1} = mV \frac{\partial W}{\partial x} \Big/ \beta\sqrt{m^2 - 1} \tag{4a}$$

Region II

$$u = u_{p2} = \frac{2}{\pi} u_{p1} \sin^{-1}\sqrt{\frac{m^2 - 1}{m^2 - a_0^2}} \tag{4b}$$

Region III

$$u = u_{p3} = \frac{2}{\pi} u_{p1} \sin^{-1}\sqrt{\frac{a_3(m+1)}{a_3 - m}} \tag{4c}$$

Region IV

$$u = u_{p4} = u_{p2} \sin^{-1}\sqrt{\frac{a_3(m+1)}{a_3 - m}} \tag{4d}$$

In the formulas of (4), the influence of the quadratic M line is neglected. For the s and λ in the formulas of (3) and (4), see Fig. 1 and in these formulas $\beta = \sqrt{M^2-1}$, M is the Mach number, $m = \beta/\mathrm{tg}\lambda$, E'(m) is the second complete elliptical

integral using $\sqrt{1-m^2}$ as the modulus, we used the "calculating-geometric mean value method" for calculations and

$$a_3=\beta y/x$$

$$a_{1,2}=y\Big/\left(\left(1+\frac{1}{m}\right)s\mp y\right)$$

$$a_3=\beta(y-s)\Big/\left(x-\frac{\beta s}{m}\right)$$

By using the $P_p(x,y,\omega)$ of formula (1) and the $P_x(x,y)$ of formula (2), this method gives the supersonic unsteady aerodynamic forces on the wing surface as

$$P(x,y;\omega)=P_p(x,y;\omega)P_o(x,y)/P_o(y) \qquad (5)$$ F.N.1

Here, $P_o(y)$ is the process numerical function and its value is

$$P_o(y)=\int_{x_L(y)}^{x_T(y)}P_o(x,y)x^{r-1}dx\Big/\int_{x_L(y)}^{x_T(y)}x^{r-1}dx \qquad (6)$$

In the formula, x_L and x_T are separately the x coordinate of the leading and trailing edges of the wing surface. In reality, by using the extended theorem of mean value, $P_o(y)$ can be viewed as the pressure of a certain x point of the span direction y section. When each point of this section has this pressure, the produced r-1 subtangent is equal to the r-1 subtangent produced by the conical flow pressure distribution. r is called the process numerical function. It reflects the calculation method for the disturbance quantity of each point on the wing surface. Based on the transonic and supersonic law of similarity to

F.N.1 Because the conditions assumed by the conical flow theory are also approximately satisfied in the flutter analysis which is primarily of the low order type, after revising the piston theory, the induced velocity produced by unsteady aerodynamic forces still approximately satisfies the boundary conditions.

suitably select similar parameters and undergo a large number of numerical tests, the formulas for the given r are:

For the subsonic leading edge, $m \leqslant 1.0$

$$r = 2 + 2\delta\left(m - 6\left(0.1A\,\mathrm{tg}\,\lambda\right)^4\right) \qquad (7a)$$

For the supersonic leading edge, $m > 1.0$

$$r = \left(1 + 4.8\delta/m\right)\left(1 + 3\delta\left(1 - \delta\right)\right) \qquad (7b)$$

Here, δ is the square root of the taper ratio and A is the aspect ratio.

III. Calculation Examples

This method is combined with the flutter automated analysis method and uses FORTRAN language on the DJS-8 computer to draw up the practical WSFA flutter analysis program. Table 1 gives the circumstances of the calculated examples. See Fig. 2 for the major initial data. The detailed initial data can be found separately in References [6-8]. These examples include four different types of plane forms as well as the situations of flat-plate wings and variable thickness wings and they are representative.

(1)例 题	(2) 机 翼 描 述	颤振计算状态(M数)(13)
1	45°平板三角翼 (3)	1.3, 2.0, 3.0
2	60°平板三角翼 (4)	1.5, 2.0, 2.5
3	70°平板三角翼 (5)	1.3, 1.64, 2.0, 2.55, 3.0
4	15°平板等弦后掠翼 (6)	1.3, 2.0, 3.0
5	30°平板等弦后掠翼 (7)	1.3, 2.0, 3.0
6	45°平板等弦后掠翼 (8)	1.3, 2.0, 3.0
7	60°平板等弦后掠翼 (9)	1.3, 2.0, 3.0
8	四分之一弦线后掠角45°，翼型NACA65A004的尖削后掠翼(10)	1.3, 2.0
9	四分之一弦线后掠角60°，翼型NACA65A004的尖削后掠翼(11)	1.3, 2.0
10	翼型为NACA65A002的梯形翼 (12)	1.3, 2.0

Table 1 Examples of calculations.

Key: (1) Example; (2) Description of wing; (3)-(5) Flat-plate delta wing; (6)-(9) Flat-plate uniform chord swept-back wing; (10) One-quarter chord line swept-back angle of 45°, tapered swept-back wing of NACA65A005 airfoil; (11) One-quarter chord line swept-back angle of 60°, tapered swept-back wing of NACA65A004 airfoil; (12) The airfoil is the trapezoidal wing of NACA65A002; (13) Flutter calculation state (M number).

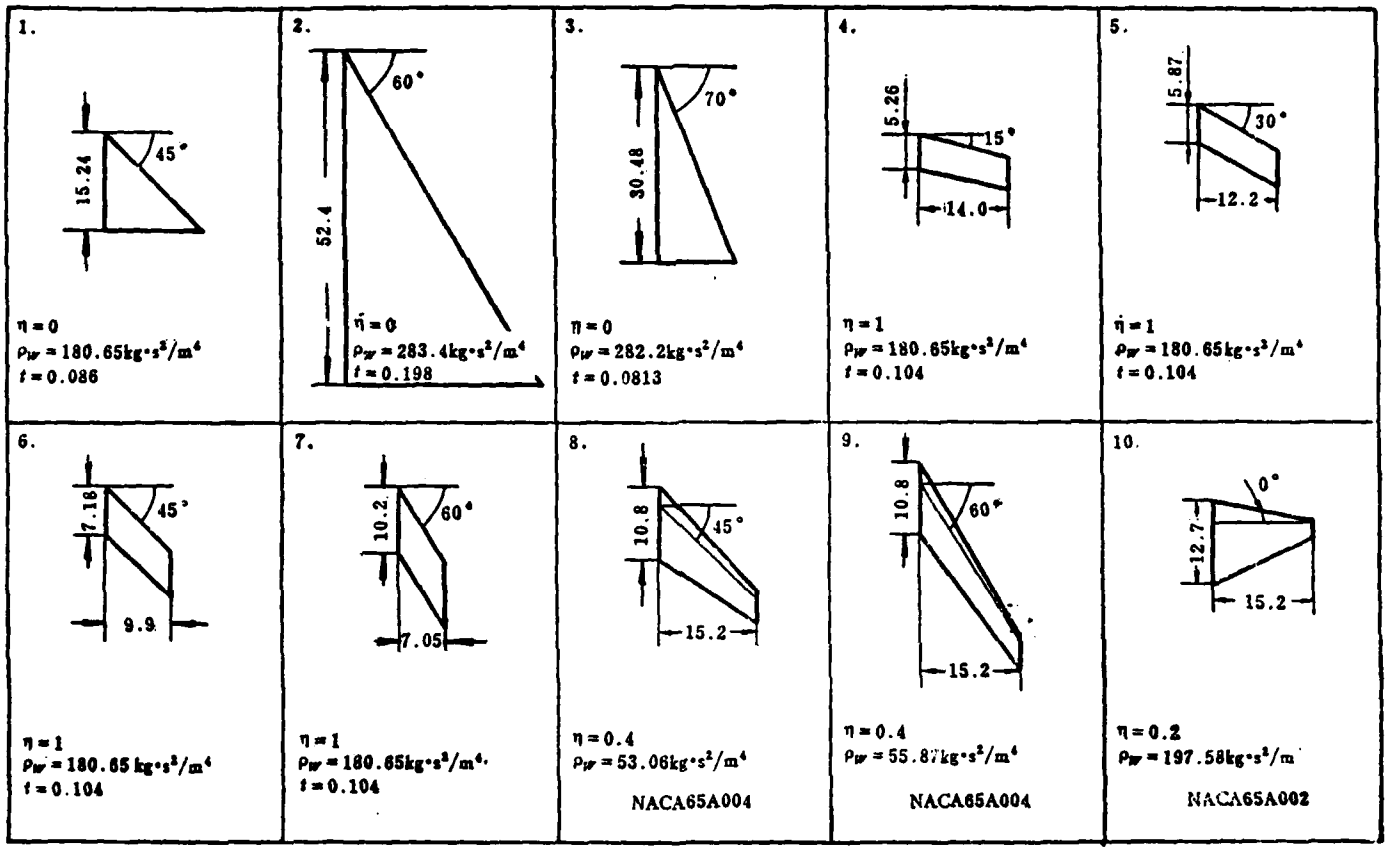

(1) 注：尺寸单位cm。例4～7中，当M = 1.3时，翼面材料密度$\rho_w = 281.16 kg \cdot sec^2/m^4$

Fig. 2 Some initial data for flutter calculation examples.

Key: (1) Note: the unit of size is cm. In test cases 4-7, when M=1.3, wing surface material density $\rho_W = 281.16 kg \cdot sec^2/m^4$.

The calculation results are compared with the flutter test data obtained in wind tunnels and they are separately given in Figs. 3-12. The figures also give the calculation results using the piston theory method (except where indicated, they were computed with the WSFA program). The quantities compared were stiffness height parameter H and the flutter frequency ratio (the ratio of calculated value $\omega_{f,c}$ and test value $\omega_{f,e}$). H is the important dimensionless quantity for determining the flutter and it is given as

$$H=\frac{(1+3\eta)\omega_\alpha}{4a}\sqrt{3W_0/\pi g\rho s(1+\eta+\eta^2)} \qquad (8)$$

Here, ω_a is the first order torsional frequency of the wing; W_o is the weight of the wing; g is the gravitational acceleration.

Figures 3-5 separately give the flutter calculation results of 45°, 60° and 70° delta wings. The test values were separately taken from References [6,7,8]. Among them, in test case 3, the H test value of M=2.0 is taken from the test curve drawn from the test values [8] but they are not taken directly from test values because these values are noticeably high. It can be seen from the figures that aside from individual points, the H values given by this method do not have more than 6% errors as compared to the test values and the errors of flutter frequency ω_f do not exceed 8%. The piston theory method also has relatively good accuracy for the flutter analysis of delta wings. The H error is generally about 15% and the error of ω_f is about 12% yet they are worse than this method.

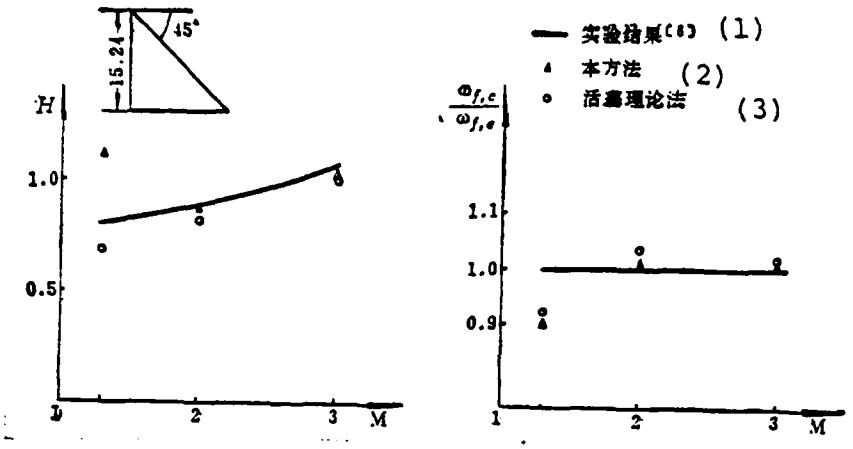

Fig. 3 Comparison of calculated and test results for test case 1.

Key: (1) Test results [6]; (2) This method; (3) Piston theory method.

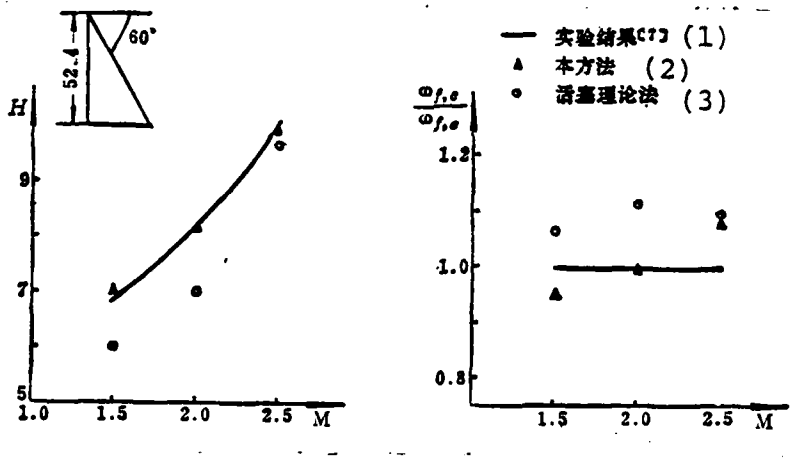

Fig. 4 Comparison of calculated and test results for test case 2.

Key: (1) Test results [7]; (2) This method; (3) Piston theory method.

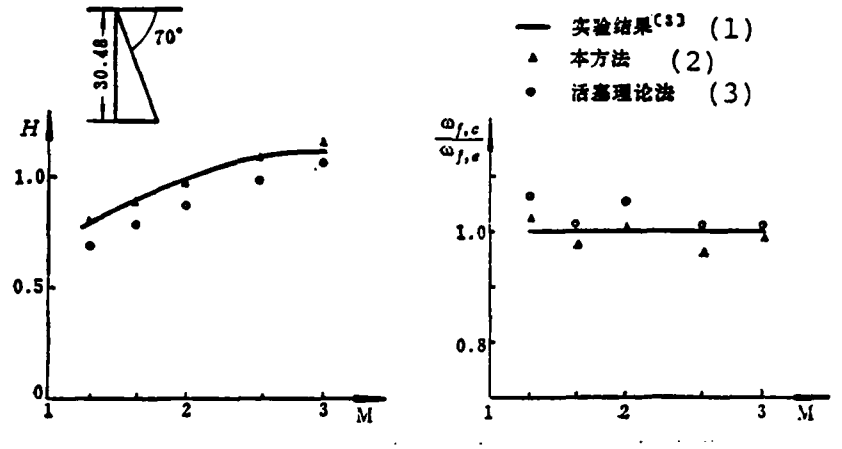

Fig. 5 Comparison of calculated and test results for test case 3.

Key: (1) Test results [8]; (2) This method; (3) Piston theory method.

Figures 6-9 give the flutter analysis results of uniform-chord flat-plate swept-back wings with swept-back angles of 15°, 30°, 45° and 60°. See Reference [6] for the test data. It can be seen from the figures that the errors of the H and ω_f values calculated by this method are not greater than 10%, the individual H values are somewhat higher and the difference reaches 19%. However, under M=1.3 conditions, the calculation value error of ω_f of each test case tends to be large, 20-30%. The reason for this is possibly because in the initial data given in Reference [6], the test model material when M=1.3 is not magnesium again but was changed to aluminum alloy. This naturally caused the calculated flutter frequency to have relatively large errors (because the influence of the change of the model material on the flutter model is relatively small). Further, in test case 7, when M=1.3 and 2.0, aside from the low frequency flutter solutions which occur in the tests, high frequency solutions also occur in the calculations. Moreover, when M=2.0, this high frequency flutter is somewhat lower than the lower frequency solution. In Fig. 9, only a comparison of the low frequency flutter solution is made. The piston theory method is

very poor for analyzing the supersonic flutter of swept-back wings. All four of these test cases were unable to calculate the low frequency flutter solution in the tests and they were only able to obtain high frequency solutions. In this way, the H values were too low, reaching more than 50% higher than the test data. The calculated values of the piston theory method given in Fig. 8 were taken from Reference [4] and in the calculations it analytically used polynominal expressions to express the test flutter model. That is, after this type of processing they were still only able to obtain high frequency solutions and the H value errors were also 15-30%. It is very clear that the accuracy of this method is much higher than that of the piston theory method.

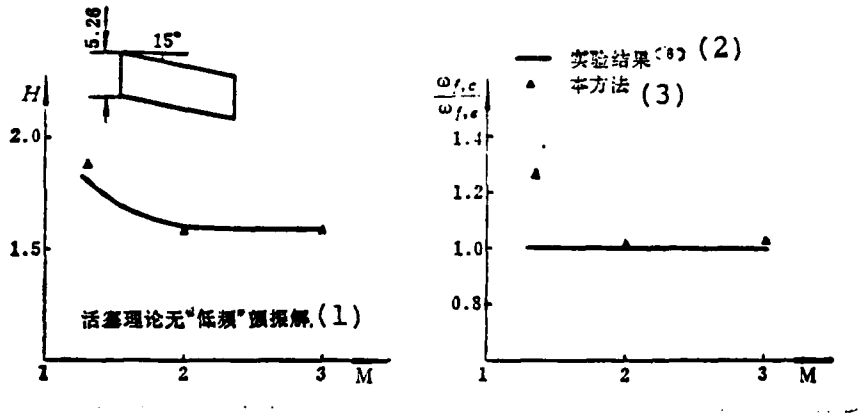

Fig. 6 Comparison of calculated and test results for test case 4.

Key: (1) The piston theory method without "low frequency" flutter solution; (2) Test results [6]; (3) This method.

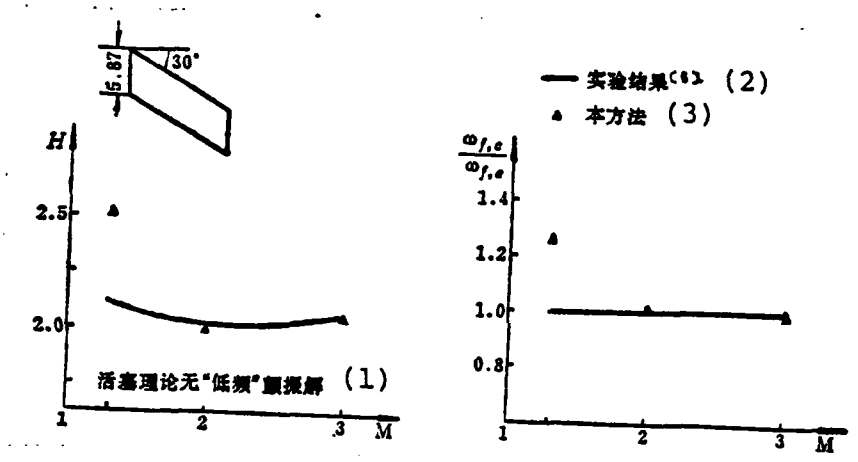

Fig. 7 Comparison of calculated and test results for test case 5.

Key: (1) The piston theory without "low frequency" flutter solution; (2) Test results [6]; (3) This method.

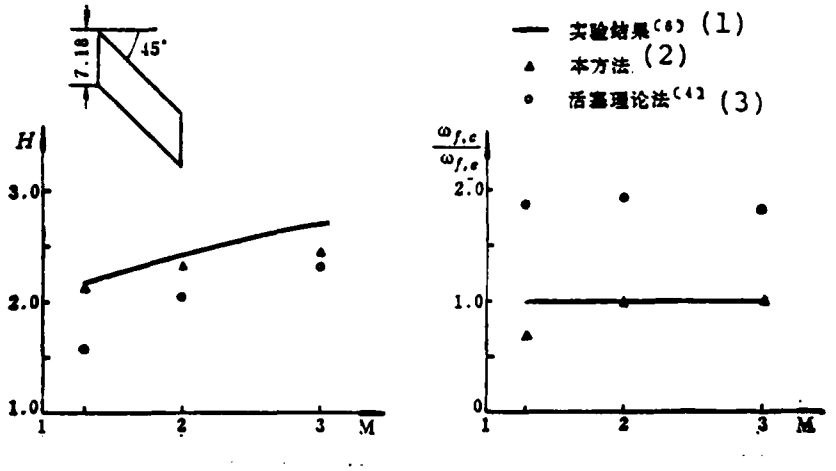

Fig. 8 Comparison of calculated and test results for test case 6.

Key: (1) Test results [6]; (2) This method; (3) Piston theory method.

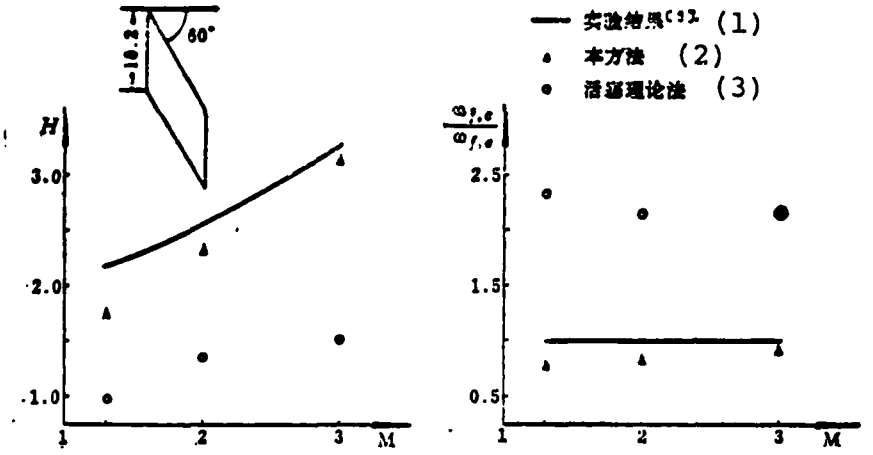

Fig. 9 Comparison of calculated and test results for test case 7.

Key: (1) Test results [6]; (2) This method; (3) Piston theory method.

Two airfoil test cases with variable thicknesses of NACA65A004, taper ratios of 0.4 and swept-back wings with one-quarter chord-line swept-back angles of 45° and 60° are given in Figs. 10 and 11. See Reference [6] for the test results.

these two test cases cannot attain flutter solution by the piston theory method but the calculation results of this method are very good. The errors of the H values and test values are not larger than 5%. The calculated value errors of ω_f in test case 9 are about 10% and the ω_f value errors of test case 8 are somewhat larger yet this is naturally much better than when using the piston theory method.

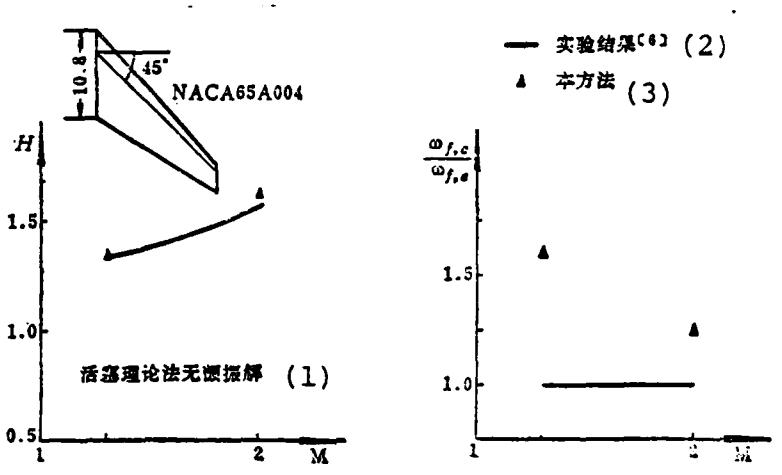

Fig. 10 Comparison of calculated and test results for test case 8.

Key: (1) Piston theory method without flutter solution; (2) Test results [6]; (3) This method.

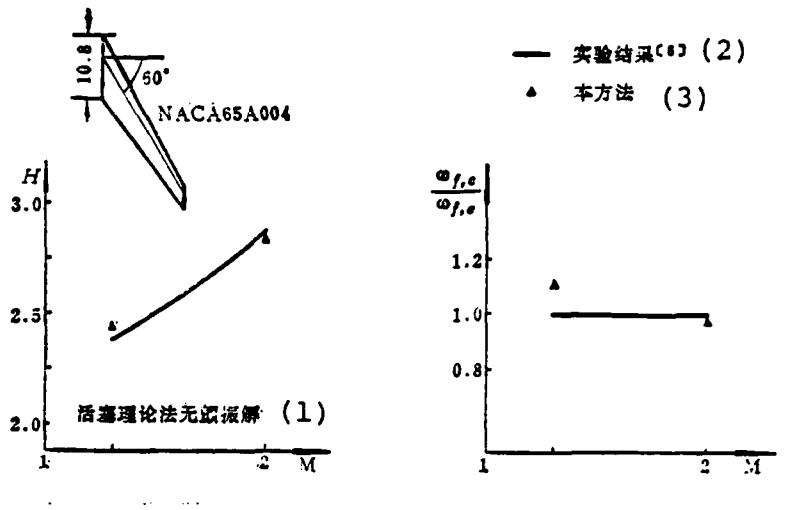

Fig. 11 Comparison of calculated and test results for test case 9.

Key: (1) Piston theory method without flutter solution; (2) Test results [6]; (3) This method.

The last test case is a variable thickness trapezoidal wing of NACA65A002, the taper ratio is 0.2 and the one-quarter chord-line swept-back angle is 0°. The test results are given in Fig. 12. The calculated results of this method are very good and when comparing the calculated values and test values [6], the H value errors are not larger than 5% and the errors of ω_f are not larger than 10%. The calculated results using the piston theory method for this type of non-swept-back trapezoidal wing are acceptable yet the H differences still reach to 40-50% and the ω_f errors are 20%.

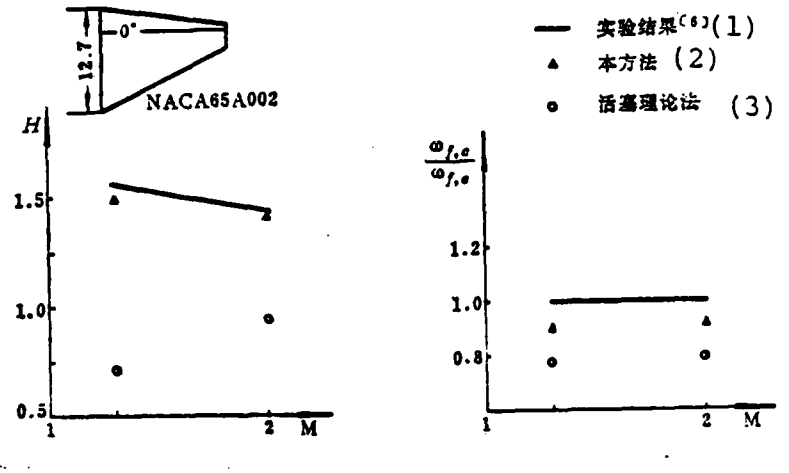

Fig. 12 Comparison of calculated and test results for test case 10.

Key: (1) Test results [6]; (2) This paper; (3) Piston theory method.

IV. Conclusion

By comparing the calculated and test data of the flutter of the above 10 test cases in 29 types of states, it can be seen that when the supersonic unsteady aerodynamic forces given by this method were used for flutter analysis, the errors were lower than 10% in comparing the great majority of obtained H values with the flutter frequency and wind tunnel flutter test results. In the flutter calculated results by the piston theory method, the H values are generally larger than 15% and often reach 40-50%. This is especially the case for the supersonic flutter analysis of swept-back wings. When using the piston theory method for calculations, it was not possible to have low frequency flutter solutions appear in the tests. However, the calculated results using this method accorded well with the test values which highlights the advantage of this method.

This method is very succinct, it does not require a great deal of computing time, it has satisfactoyr accuracy and it can

be used for model design units.

I would like to express my deep gratitude to comrade Zhang Hanxin for his guidance and help and to comrade Wang Hongzhi for his valuable views proposed for formula (7) in this paper.

References

[1] Li, T., "Aerodynamic Influence Coefficients for an Oscillating Finite Thin Wing in Supersonic Flow," JAS, Vol. 23, No. 7, 1956.7.

[2] Cunningham, A.M., Jr., "Oscillatory Supersonic Kernel Function Method for Isolated Wings," J. of Aircraft, Vol. 11, No. 10, 1974.10.

[3] Giesing, J.P. and Kalman, T.P., "Oscillatory Supersonic Lifting Surface Theory Using a Finite Element Doublet Representation," AIAA Paper 75-760, 1975.5.

[4] Morgan, H.G., Huckel, V. and Runyan, H.L., "Procedure for Calculating Flutter at High Supersonic Speed Including Camber Deflection, and Comparison with Experimental Results," NACA TN 4335, 1958.9.

[5] Zeng Weiqin and Wang Xianxin, "Automated Method for Determining the Flutter Velocity and the Flutter's Critical Point Gas Flow Density," Chinese Aerodynamic Research and Development Center, 1977.12.

[6] Tuovila, W.J. and McCarty, J.L., "Experimental Flutter Results for Cantilever-Wing Models at Mach Numbers up to 3.0," NACA RM L55 E11.

[7] Li Qing, "Supersonic Flutter Tests of 60° Delta Wing Flat-Plate Models," Internal Test Report of Chinese Aerodynamic Research and Development Center, 1980.4.

[8] Hanson, P.W. and Levey, G.M., "Experimental and Calculated Results of a Flutter Investigation of Some Very Low Aspect-Ratio Flat-Plate Surfaces at Mach Numbers from 0.62 to 3.00," NASA TN D-2038, 1963.10.

EFFECT OF A SHEAR LAYER ON THE STABILITY OF AN AXISYMMETRICAL EXTERNAL COMPRESSION AIR INTAKE

Zhang Kunyuan, Yu Shaozhi and Peng Chengyi
Nanjing Aeronautical Institute

Abstract

This paper discusses the effect of six shear layers with strengths of 5-11% and variable central cone external compression air intake on the stability of air intake when the intake lip is in various positions under incoming flow M=1.72 conditions.

Tests prove that when a shear layer with strength less than 10% enters near an axisymmetrical air intake this does not cause separation of the boundary layer from the inside of the air intake cowl; shear layers with strengths up to 11% can enter this air intake at any position in the area of the inlet and not produce buzz. The references showed that shear layers with strengths of only 6-7% can bring about buzz of the two dimensional air intake which reveals that the axisymmetric air intake has relatively strong resistance capabilities against the buzz caused by the shear layer intake.

I. Introduction

The stable operating range of a supersonic air intake under subcritical conditions is an important area of its performance. In the last several decades, many researchers have proposed their own views on this research. This paper studies the effect of the intake of a shear layer on the stability of an axisymmetrical external compression air intake.

The shear layer theory of Ferri is generally accepted and it has also been verified by a great number of experiments [1].

This theory points out that when the shear layer formed from the intersection of shock waves enters the air intake near the lip, it possibly promotes the separation of the boundary layer from the inside of the cowl and causes air intake buzz. This is the famous Ferri criterion.

At the end of the 1960's, Fisher et al of England successfully used the Ferri criterion in a two-dimensional air intake when developing the "Harmony" model [2]. They pointed out that a shear layer with strength lower than 6-7% could cause buzz when entering the air intake near the inside of the lip. The definition of this strength is the ratio of the total pressure difference of the air flow on the two sides of the shear layer and the total pressure of the upstream air flow on the shock wave's convergent point. The report also proves that the tendency of the inner wall air flow separation of the cowl is to become stronger with the strengthening of the strength of the shear layer and weaken with the enlargement of the distance of the shear layer from the cowl.

There is no doubt that the research of Fisher et al is very valuable for two-dimensional air intakes. However, it is unable to directly resolve the analogous problem of the axisymmetrical air intake. These two types of air intakes have very great differences in the reaction level of the shear layer and other important details. This paper is aimed at the effect of using a common axisymmetric air intake to specially research a shear layer on its subcritical stability.

II. The Shear Layer of a Typical Biconic Air Intake

We researched a double cone with a maximum incoming flow M number of 2.2. The cone semi-angles of the first and second cones of the air intake central cone are separately 17.5% and 25%. When the incoming flow M number is 2.2 the first intake's oblique wave is sealed, when $M < 2.2$ we let the second intake's

wave be sealed and when the M number is between 1.8-2.2, theoretically the inlet wave system has the following several situations under critical and subcritical operations: 1. critical; 2. slightly subcritical; 3. relatively large subcritical (Fig. 1).

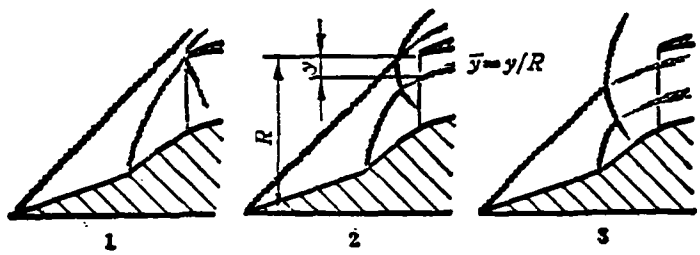

Fig. 1 Several types of inlet wave systems of biconic air intakes.

We will now calculate how large the produced shear layer's strength is based on the structures of the above wave systems.

The definition of the shear layer's strength S_v is

$$S_v = \frac{\text{total pressure difference on both sides of shear layer}}{\text{total pressure of incoming flow x 100\%}}$$

The calculation results are shown in Fig. 2. Aside from this, distance y of the two intake wave's shear layers from the lip (or relative distance $\bar{y}$) is an important factor for determing the size of the effect of the shear layer. It is the function of the M number and flow coefficient φ. See Fig. 3.

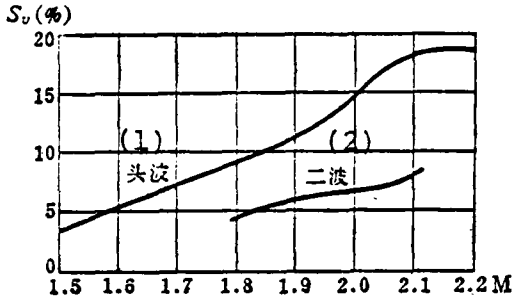

Fig. 2 Relationship of S_v to the M number.
Key: (1) Head waves; (2) Two waves.

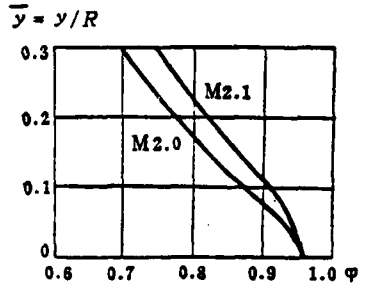

Fig. 3 Relationship of two wave shear layer distance $\bar{y}$ and flow coefficient φ.

It can be seen from the above calcuations that in the M=1.8-2.1 range, the shear layer of the biconical air intake has the following most basic situation with two points:

(1) The shear layer of the head waves is relatively strong and its strength is 8.8-17.8%. However, this relatively strong shear layer cannot enter the lip near the critical state but can only enter after being in a relatively strong subcritical state;

(2) The shear layer strength of two intake waves is about 4.8-8%. It can enter the lip beginning in the subcritical, its maximum value is located in the situation whereby flow coefficient $\varphi < 0.9$ and at this time distance $\bar{y} > 0.9$.

When analyzing the test materials published abroad, we noticed that the weakest shear layer which was able to cause the axisymmetric external compression air intake to buzz had a strength of 14.2% [3]. Based on this situation, it can be considered that in the air intake which we analyzed, a shear layer with strengths greater than 14.2% should not be allowed to enter the lip. This paper focuses research on the relationship of a shear layer with strength lower than 14.2% but much higher than the 6-7% given by Fisher and the stability of an axisymmetrical air intake.

III. Test Model and Equipment

We used a single cone external compression air intake model with variable cone angle and adjustable cone axial position and carried out shear layer function tests in an M-1.72 free jet flow wind tunnel. This model can produce shear layers with strengths of 5.2%, 6.1%, 7.9%, 9.1%, 10.2% and 11% and can also enter the lip under various distance y. The model's inlet diameter is ϕ 106mm, the wind tunnel's test section is 300x300mm and the test which used the model's inlet diameter for calculation had $Re \approx 2 \times 10^6$. The model arranged along the flow has four dynamic pressure sensors and total and static measuring holes to measure the related static and dynamic parameters under various conditions. See Fig. 4 for a sketch of the model.

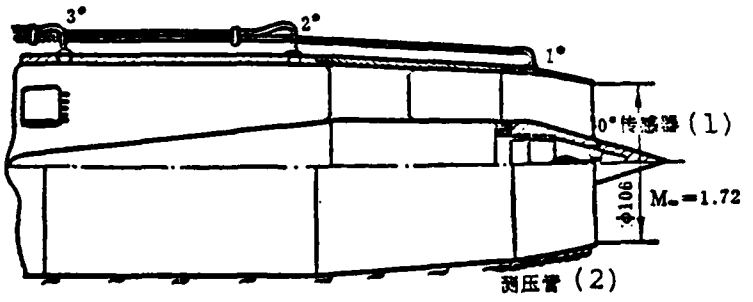

Fig. 4 Model of air intake.
Key: (1) Sensor; (2) Piezometric tube.

IV. Test Results

(1) After a shear layer with strength up to 11% enters the lip, the static pressure fluctuation of the air intake's outlet section does not noticeably change.

We separately placed six different cones in cone wave sealed design cone positions and during testing allowed the shear layer with six different strengths to go from not entering to entering the air intake near the air intake lip. At the same time, we investigated whether or not the operating conditions of the entire air intake had any noticeable changes, especially changes in the static pressure fluctuation of the outlet section. Results showed that when these six cones with different strengths entered the air intake near the lip, the air intake did not have any signs of buzz. The buzz began in the air intake only when the positive shock waves were pushed very far from the lip, that is, the positive shock waves began to have noticeable vibration and the outlet's static pressure fluctuation had noticeable enlargement. In brief, a maximum stable subcritical condition existed. See Table 1.

内 容(1) \ (2) 锥角 δ_c	27°	24°	20°	18°	16°
(3)试验时滑流层强度 S_v %	11.2	10	9.4	7.8	6.1
(4)正激波最大稳定距离(距唇口)(mm)	11	1.	13	5	4
(5)此状态下流量系数 φ	0.94	0.95	0.91	0.96	0.96
(6)此状态下滑流层距离 y_M(mm)	5.3	8.1	8.2	3.6	3.0
(7)滑流层进入前出口压力脉动 $\frac{\Delta p_M}{p_{0_\infty}}$ %	1~2	1~2	1~2	1~2	1~2
(8)滑流层进入后出口压力脉动 $\frac{\Delta p_M}{p_{0_\infty}}$ %	1~2	1~2	1~2	1~2	1~2

Table 1 Parameters when there is maximum subcritical operation.
(continued next page)

Table 1 (continued)

Key: (1) Contents; (2) Cone angle; (3) Shear layer strength during testing; (4) Maximum stable distance (from lip) of positive shock wave; (5) Flow coefficient under this condition; (6) Shear layer distance under this condition; (7) Outlet pressure pulsation before shear layer enters; (8) Outlet pressure fluctuation after shear layer enters.

Figure 5 shows the curves of the outlet static pressure fluctuation of a 24% cone model. When $1 > \varphi > 0.93$, although a shear layer with strength of 10.7% has already entered the lip, yet the situation of the pressure fluctuation and subcritical operations do not have noticeable changes.

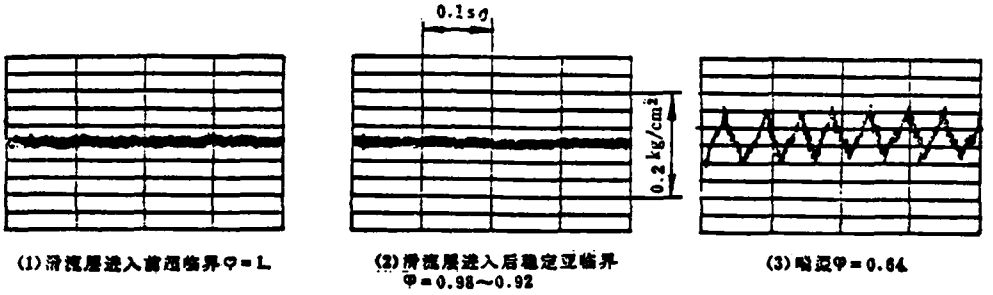

Fig. 5 Changes in the pressure fluctuation at outlet section of 24° cone.

Key: (1) Supercritical operation before shear layer enters; (2) Stable subcritical operation after shear layer enters; (3) Buzz.

In brief, when the air intake begins to have noticeable unsteady flow, with good reason we consider that this unsteady flow was not created by the shear layer but possibly from the separation of the boundary layer from the central body.

(2) The Strongest Shear Layer Does Not Have Buzz When Entering the Inlet at Different Distances From the Lip

We employed two methods to control entering distance y of

the shear layer. The first is to gradually shrink into the central cone to maintain a critical state. The second method is to gradually push the positive shock waves out towards the cone tip under a certain fixed cone position. In this way, distance y of the shear layer from the lip gradually increases and gradually approaches the central cone. We will now list a set of test results of the strongest shear layer in the following table:

(1) 试验方法	(5) 逐步缩入中心锥，保持临界工况								(6) 中心锥固定逐步向外推出正激波
(2) 滑流层距离 y(mm)	0	2	3	4	5	7	7.4	10.5	10.5～35
(3) 出口静压脉动 $\frac{\Delta p_4}{p_{0_\infty}}$%	1～2	1～2	1～2	1～2	1～2	1～2	1～2	1～2	1～2
(4) 进气道工作情况	(7) 无任何喘振迹象								

Table 2 Test results of the strongest shear layer entering the air intake at different distances from the lip.

Key: (1) Test method; (2) Shear layer distance; (3) Outlet's static pressure fluctuation; (4) Air intake's operating condition; (5) Gradually shrinks into the central cone to maintain a critical state; (6) The central cone is fixed and gradually pushes outwards towards the positive shock wave; (7) No signs of buzz.

This shear layer did not produce buzz when entering our test air intake on various positions of the lip section.

We did similar tests on shear layers with five types of strength and the results were similar. Therefore, no matter from what distance the studied shear layers with six types of strengths entered the lip, they were unable to induce buzz in the air intake.

(3) Characteristics of Air Flow Separation Inside the Cowl

It is generally considered that the buzz caused by the

entering of the shear layer was due to the separation of the boundary layer inside the intake cowl. Therefore, the existence of a separation region brings about the necessary conditions for this type of unsteady flow. In this test, we paid attention to the fact that the shear layer had no capability to cause the air intake to enter buzz operations and it was thus necessary to see whether or not these shear layers had caused separation inside the cowl. For this reason, we conscientiously researched the characteristics of the air flow separation inside the cowl after different strength shear layers entered the lip at different distances. Figure 6 gives the test results. There are a total of 16 test points on the figure and when the strength was smaller than 10%, 7 test points did not have air flow separation in the lip, the corresponding static pressure fluctuation of the outlet section did not show any abnormal areas and the pressure fluctuation amplitude was only 1-2% incoming flow total pressure.

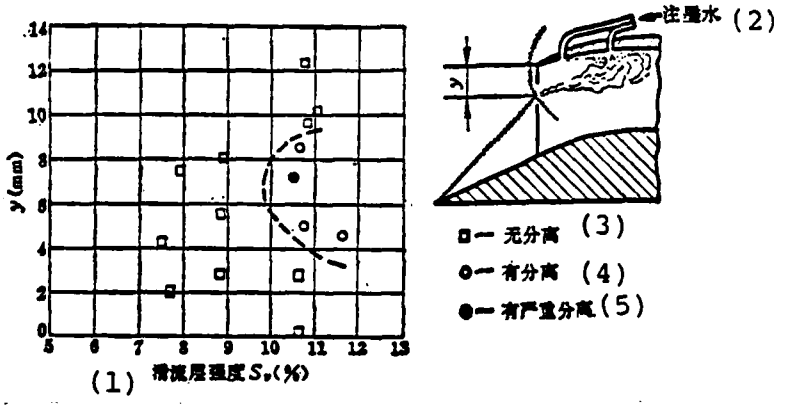

Fig. 6 The relationship of shear layer strength S_v and distance y and the lip separation.

Key: (1) Shear layer strength; (2) Pour in ink;
(3) Without separation; (4) With separation;
(5) With serious separation.

When the strength was greater than 10%, among 9 test points, lip separation occurred 4 times and among these the lip separation of one point was especially serious. Its S_v=10.6%, y ≈ 7.4mm

and yet it had an extremely large separation region and the model's outlet static pressure was still very small (see Fig. 7). This shows that when the air flow separation has not yet created serious blockage, it is not sufficient to induce buzz.

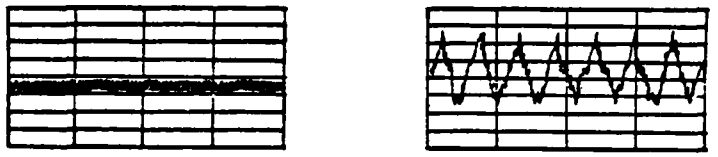

(1)24°锥, S_v=10.6%, y=7.4mm 唇口有严重分离时出口压力脉动

(2)24°锥啸振时出口压力脉动

Fig. 7 Outlet pressure fluctuations of 24° cone model without and with buzz.

Key: (1) 24° cone, S_v=10.6%, y=7.4mm, the outlet pressure fluctuations when the lip has serious separation; (2) Outlet pressure fluctuations when 24° cone has buzz.

Secondly, we noticed that the shear layer had the most noticeable operating distance. Outside the $y \approx$ 5-9mm range, shear layers with strengths of 11% are still unable to cause boundary layer separation. In the tests, the most noticeable operating distance $\bar{y} = \frac{y}{R}$=10-18%.

These tests proved that shear layers with strength S_v=11% cannot damage the axisymmetric air intake. It can therefore be anticipated that we must cause the shear layer strength of the Ferri type unsteady flow to be higher than 11% in the axisymmetric air intake.

Naturally, it is not an easy question to resolve how large a shear layer strength a specific air intake can sustain and it is related to other factors. Therefore, the results obtained from these tests naturally cannot be viewed as an absolute criterion. However, based on our test results and the published two-dimension air intake test results, the ability of axysymmetric air intakes to endure shear layers must be stronger than

two-dimensional air intakes.

V. Conclusion

(1) The strength of a shear layer must be somewhat larger than 10% to be able to cause separation of the boundary layer inside the cowl of an air intake. However, if the separation of the boundary layer does not produce serious blockage, it is not sufficient to induce buzz.

(2) Only if a shear layer enters at a place a suitable distance from the lip can it cause the most marked air flow separation effect. In these tests, this distance was equal to 10-18% of the inlet's radius, that is, 5-9mm.

(3) Shear layers with strengths less than 11% which enter axisymmetric air intakes are unable to cause the air intake to buzz. The axisymmetric air intake can sustain even higher strength shear layers than the two-dimensional air intake.

References

[1] A. Ferri and L.M. Nucci, The Origin of Aerodynamic Instability of Supersonic Inlets at Subcritical Conditions, NACA RM L50 K30, Jan. 1951.

[2] S.A. Fisher, M.C. Neale, A.J. Brooks, On the Sub-critical Stability of Variable Ramp Intakes at Mach Number Around 2, ARC R8M3711, 1970.

[3] D.G. Stewart, Supersonic Diffuser Instability-the Effect of Design Geometry on Intakes of 25% Cone Semi-angle at M1.83, ARL Report ME104, 1962.

COMMENT ON "DETERMINATION OF AERODYNAMIC COEFFICIENTS FOR A REENTRY BODY BY MEANS OF THE KALMAN FILTER METHOD"

Cai Jinshi
Chinese Aerodynamic Research and Development Center

Abstract

The comment emphatically indicates that a mathematical model for aerodynamic parameter identification of a reentry body bases only on the data of angular rates and accelerations onboard but not on trajectory observation data, as stated in the paper, it can only determine the ratio between aerodynamic coefficients of the reentry body but can't determine the aerodynamic coefficients directly.

In the latest issue of the Journal of Aeronautics, Vol. 3, No. 3, comrade Jiang Quanwei et al proposed that in situations without orbitally observed data, by only relying on data of accelerations and angular rates measured on the aircraft, we can determine the aerodynamic coefficients for a reentry body by means of the Kalman filter method. For this topic, I proposed different views and discussed them with comrade Jiang Quanwei and others. I consider that: the mathematical model established by this paper to determine aerodynamic coefficients cannot be identified; when there is no orbitally observed data and we only rely on data measured by accelerations and angular rates, we can only determine the ratio of aerodynamic coefficients for a reentry body but we are unable to accurately determine aerodynamic coefficients.

The system identification theory tells us that for the mathematical model of a system identification, if there is one-to-one correspondence of the images from the parametric space to the model's input-output space, this type of model is identifiable.

If there are many different sets of parameters corresponding to the same input-output relationship for the mathematical model of certain system identification, then this model is not identifiable.

The parametric space of this paper's system identification mathematical model is composed of the unestimated value of aerodynamic coefficient $\underline{C}$ and the state variable initial value ($\underline{X}_o$, H_o). Rudder angle $\underline{\delta}$ is known and is the system input. Because this model relies on accelerations and angular rates to carry out identification, the output of the system is ($\tilde{N}_x$, $\tilde{N}_y$, $\tilde{N}_z$, p, q and r). This is easy to verify.

For this system, numerical group A($\underline{C}$, $\underline{X}_o$ and H_o) and data B($\underline{C}\exp(\Delta H_o/k_o)\underline{X}_o$, $H_o + \Delta H_o$) of the parametric space correspond to a similar input-output relationship and therefore the group of parameters is not identifiable.

By only relying on data of acceleration and angular rates, we cannot determine that the aerodynamic coefficients have physical significance. Aircraft movement is determined by the force and moment acting on the aircraft; aircraft movement parameters (accelerations and angular rates) can also in turn determine the force and moment on an aircraft. However, aerodynamic force and moment are a function of the product of the aerodynamic coefficient and the dynamic pressure Q. For aircraft with similar initial states, different aerodynamic coefficients only require that it have the same product as the dynamic pressure to be able to have similar aerodynamic force and moment and thus have the same accelerations and angular rates. Therefore, by only relying on accelerations and angular rates, if there is no new additional information to separate out the dynamic pressure, then there will be no way to determine the aerodynamic coefficient. This is the physical nature of things and cannot be resolved by a mathematical method (e.g. Kalman filter).

By only relying on the data of accelerations and angular rates, we are only able to determine the ratio of the aircraft's aerodynamic coefficients. Naturally, if we are able to determine a certain aerodynamic coefficient, we can also determine other aerodynamic coefficients.

From formula (9) of the paper we can obtain

$$Q=[\tilde{N}_{xg}+X_1 m(g^2+r^2)]/(c_{x_0}S)\equiv(N_{xg})/(c_{x_0}s)$$

By substituting the above formula into formulas (8) and (9) of the paper, we can obtain a new set of state equations and a set of observational equations. Its undetermined aerodynamic coefficient is

$$\underline{C}=\left(\frac{c_{y\beta}}{c_{x_0}},\ \frac{c_{ybr}}{c_{x_0}},\ \frac{c_{z\alpha}}{c_{x_0}},\ \frac{c_{zbp}}{c_{x_0}},\ \frac{c_{lp}}{c_{x_0}},\ \frac{c_{lr}}{c_{x_0}},\ \frac{c_{m\alpha}}{c_{x_0}},\ \frac{c_{mq}}{c_{x_0}},\ \frac{c_{mbq}}{c_{x_0}},\ \frac{c_{n\beta}}{c_{x_0}},\right.$$

$$\left.\frac{c_{nr}}{c_{x_0}},\ \frac{c_{nbr}}{c_{x_0}}\right)^T.$$

The state equations and observational equations of this mathematical model do not include dynamic pressure Q and height H. Therefore, it is not necessary to have orbital parameters and by using the maximum likelihood method or Kalman filter method we can identify the ratio of the aerodynamic coefficients but cannot identify the aerodynamic coefficients.

This paper used the generalized Kalman filter method and used the aerodynamic coefficient's filter convergence value as the determined aerodynamic coefficient value. Because of the unidentifiability of these coefficients, the initial filter value of the filter convergence value and state parameters as well as the initial covariance value are related. Simulated calculations show that by changing these initial values, the determined aerodynamic coefficients will also be different. It is only necessary for these initial values to slightly allow modification and then the errors of the main determined aerodynamic coefficients

can reach above 20%. Therefore, when resolving in situations without orbitally observed data spoken of in this paper, it is not precise to only rely on the data of accelerations and angular rates to determine coefficients.

THIRD NATIONAL CONFERENCE OF THE AERONAUTICAL SOCIETY OF CHINA

The Aeronautical Society of China held its Third National Conference in Xian from March 24 to 28 in 1983. Nearly 300 representatives from aeronautical and aerospace production, utilization, scientific research and mathematics departments from various districts of China attended the conference. The conference listened to and deliberated on the work report of the Second Council, discussed the passage of the new constitution and employed the secret ballot method to select a new council. Wei Wenmei was elected as director and Gao Zhenning, You Jiang, Yao Jun, Wang Wanlin, Li Ming, Zhuang Fenggan, Cao Chuandiao and Zhang Azhou were elected as deputy directors and Wang Nanshou was elected as secretary-general.

The standing council approved inviting Cao Lihuai, Mei Jiasheng and Shen Yuan as advisers to the Aeronautical Society of China.

AERONAUTICAL SOCIETY OF CHINA HOLDS ITS "SECOND ACADEMIC EXCHANGE CONFERENCE ON ENGINE STRUCTURE, STRENGTHS AND VIBRATIONS"

The Aeronautical Society of China convened its "Second Academic Exchange Conference on Engine Structure, Strengths and Vibrations" in Wuxi in Jiangsu Province from April 21 to 25 of 1983. The conference representatives were over 140 persons from a total of 46 units of the airforce, navy, civil aviation, the Ministry of the Aerospace Industry, the Ministry of the Aviation Industry, the Ministry of the Machinery Industry, factories attached to the Chinese Academy of Sciences system and related institutions of high education from throughout China. The conference received 106 academic papers and reports, 73 of which were read at the conference and there were also two specially invited reports.

The papers and reports read at the conference were all concerned with the newest achievements in application research in the fields of engine structural design, strength and vibration, materials and material strength etc. They prominently showed the advancements in recent years in the fields of aviation engine structural integration and aviation engine developed programs, engine load spectrum and lifetime calculation research, engine materials and materials research etc. Related experts were also invited to the conference to present comprehensive reports on the state of present domestic and foreign technical advancements and these experts were welcomed by the representatives.

During the conference, separate symposiums by factories, research institutes and institutions of higher learning were held on the problems surrounding future developments in engine structures, strength and vibrations and a special symposium on high temperature fatigue strength was also held. During the conference, the formal establishment of "Engine Structure, Strength and Vibration Special Group of the Special Committee

on Dynamics of the Aeronautical Society of China was declared and the first working conference of the group was convened.

THE AERONAUTICAL SOCIETY OF CHINA HOLDS ITS "ACADEMIC CONFERENCE OF AVIATION METAL CEMENTING"

The Aeronautical Society of China convened the "Academic Conference of Aviation Metal Cementing" in Tongan County in Fujian Province from April 11 to 15 of 1983. The conference representatives included over 100 persons from 47 units of the airforce, navy, civil aviation, the Ministry of the Aerospace Industry, the Ministry of the Aviation Industry, the Ministry of Petrification, factories attached to the Chinese Academy of Sciences system, research institutes and related institutions of higher education. The conference received a total of 48 papers and reports and among these 10 were read at the plenary session.

The papers and reports read at the conference were all concerned with the newest achievements in application research and experimental research in the fields of cementing structural design, cementing techniques, adhesive materials and detection techniques etc. They basically reflected the present advanced level of China's metal cementing technology. Related experts were also specially invited to the conference to present comprehensive reports on the state of present domestic and foreign technical advancements in cementing technology. They also showed scientific and technical films related to technical advancements in cementing technology and thus invigorated scientific thoughts, widened scientific outlooks and this was inspiring to the representatives and received their unanimous favorable comments. The conference also carried out specialized discussions of present problems existing in the development of China's metal cementing technology and future development trends and they also proposed consultative recommendations to related departments.

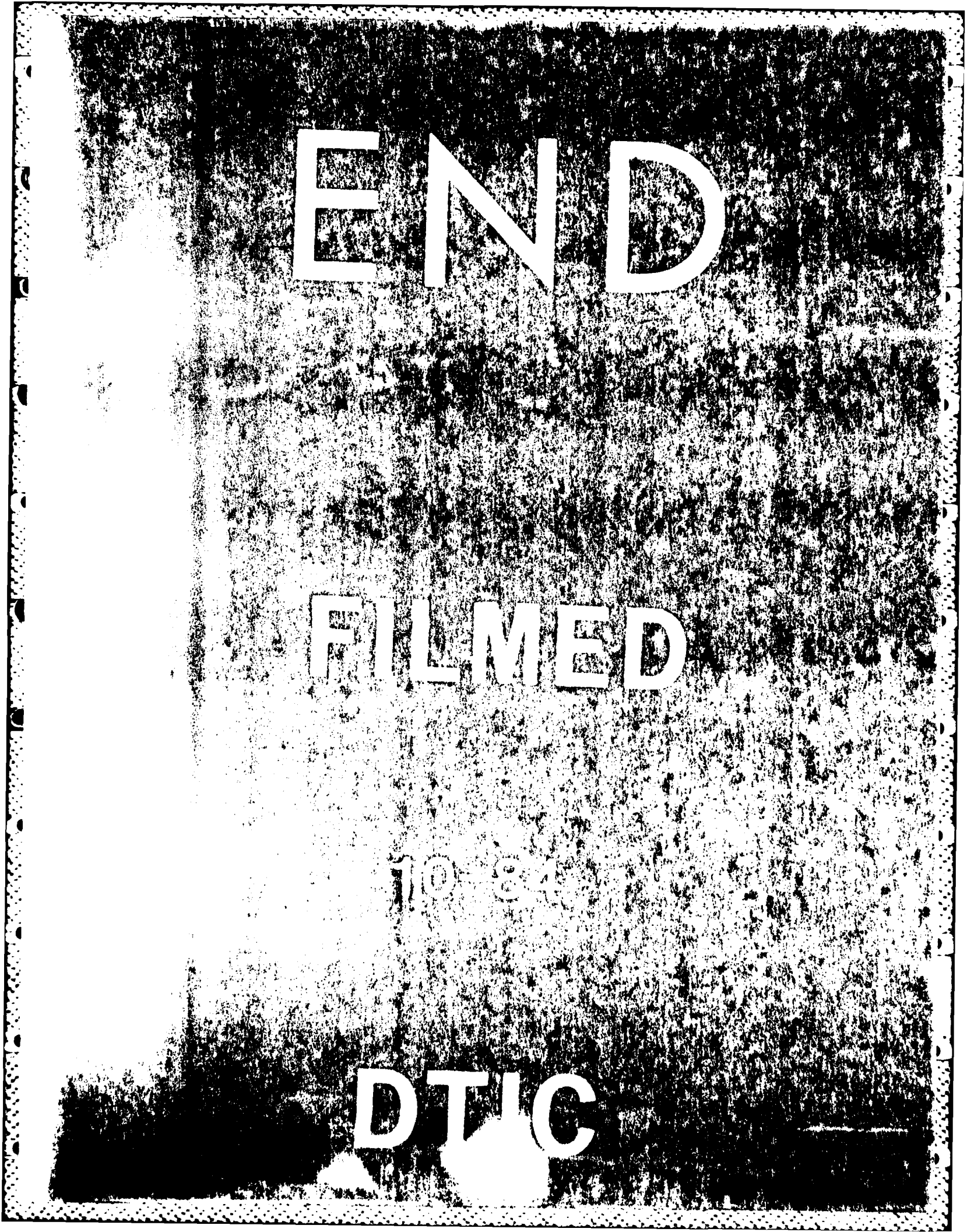
END
FILMED
DTIC